

Propagation of future climate conditions into hydrologic response from coastal southern California watersheds

Dongmei Feng ¹ • Edward Beighley ^{1,2} • Roozbeh Raoufi ¹ • John Melack ³ • Yuanhao Zhao ¹ • Sam Iacobellis ⁴ • Daniel Cayan ⁴

Received: 4 April 2018 / Accepted: 9 January 2019 / Published online: 29 January 2019 © Springer Nature B.V. 2019

Abstract

As a biodiverse region under a Mediterranean climate with a mix of highly developed and natural watersheds, coastal Santa Barbara County (SB), located in southern California, is susceptible to the hydrologic impacts of climate change. This study investigates the potential changes in hydro-meteorological variables in this region as well as their societal and ecological implications for projected climate conditions during the twenty-first century. Daily streamflow ensembles from 135 coastal watersheds for the period 2021–2100 are developed using the Hillslope River Routing (HRR) model forced with downscaled precipitation and temperature projections derived from 10 climate models in the Coupled Model Inter-Comparison Project, Phase 5, and two emission scenarios (Representative Concentration Pathways, RCP, 4.5 and 8.5). Analysis of the projected ensemble precipitation and streamflow series relative to historical conditions (1961–2000) shows (i) minimal change in annual precipitation (median change within ±3%); (ii) an altered seasonal rainfall distribution with a decrease in rainfall at the beginning of the rainy season (Oct-Dec), an increase during the Jan-Mar period, and a decrease at the end of the season (Apr-Jun); (iii) increases in the magnitude and frequency of large storms (> 36 mm/day) which combined with a shorter rainy season, lead to increases in annual peak flows; and (iv) the propagation of the altered precipitation characteristics resulting in nonlinear changes in the magnitude and variability of annual maximum discharges (i.e., mean, standard deviation, skew) impacting estimated return period discharges (e.g., estimated 100-year flood discharges for the period 2061–2100 under 8.5 increase by up to 185%). While these results are specific to southern coastal California, the nature of nonlinear hydrologic response to altered precipitation characteristics underscores the value of regional studies investigating potential impacts of climate projections on streamflow dynamics.

Electronic supplementary material The online version of this article (https://doi.org/10.1007/s10584-019-02371-3) contains supplementary material, which is available to authorized users.

☑ Dongmei Feng dmei.feng@gmail.com

Extended author information available on the last page of the article.



1 Introduction

Civil infrastructure, such as stormwater drainage systems and flood control structures, plays a major role in maintaining the functionality of modern society by (i) reducing and safely conveying runoff from agricultural and urban areas to receiving water bodies or treatment plants, (ii) protecting people, property, and associated infrastructure from riverine flooding, and (iii) avoiding or mitigating adverse impacts of urbanization on downstream water systems. The design and management of this infrastructure are dependent on our understanding of local rainfall-runoff behavior. Generally, minor urban drainage systems (e.g., road swales, curb gutters and catch basins) are designed to transport or mitigate peak runoff magnitudes for events with return periods of 2-5 years; while major flood control facilities (e.g., bridges, dams, reservoirs, and water diversions) are designed for managing storm events with return periods ranging from 50 to 100 or more years (Rosenberg et al. 2010). These design discharges are estimated by applying empirical formulas or statistical analyses based on historical synoptic and hydrologic records as well as the hydrologic characteristics of the target catchments. The underlying assumption of these off-the-shelf methods is the stationarity of hydro-meteorological processes which is often not valid when climate changes (Beighley and Moglen 2002; Beighley and Moglen 2003; Milly et al. 2008; Brown 2010). If a changing climate alters precipitation magnitudes and frequencies, the flood discharge regime will also be altered (Olsson et al. 2009; Ray et al. 2016; Hossain et al. 2015; Tamaddun et al. 2016). If the resulting changes lead to increased flood magnitudes, there will be an increased risk of failure or insufficient capacity for existing stormwater facilities to adequately convey runoff (Thakali et al. 2016). O'Neill (2010) suggests that the flood control systems designed during 1950-1970 are generally undersized for today's conditions as a result of climate change. For example, a structure designed for the 100-year discharge in 1950-1970 may only convey the discharge resulting from a 60- to 80-year event today.

In addition to the impacts on infrastructure, climate change can also impact the coastal ecosystem. The terrestrial export of water into the coastal zone (i.e., estuaries and other coastal marine environments) can be an important source of nutrients and sediments (Brzezinski et al. 2013). The Santa Barbara Channel, located offshore of SB, provides excellent habitats for giant kelp forests and associated diverse ecosystems. Winter storms and the resulting runoff are sources of sediments and nutrients to these coastal ecosystems, making these ecosystems susceptible to variability in hydro-meteorological conditions (Beighley et al. 2003; Beighley et al. 2008; Goodridge and Melack 2012; Warrick et al. 2015). For example, the projected increase in the frequency of extreme storms may lead to significant decreases in foundational species and thus reduce the diversity and complexity of kelp forest food webs (Byrnes et al. 2011). Therefore, investigating how future climate conditions influence terrestrial export is essential for understanding coastal ecosystems and enabling climate adaptation planning (Myers et al. 2017).

Climate and associated hydrologic conditions in the southwestern US have changed over the twentieth century. A temperature increase diminished mountain snowpack and an earlier onset of snowmelt have been identified (Barnett et al. 2008; Bonfils et al. 2008; Pierce et al. 2008; Hidalgo et al. 2009; Mishra and Lettenmaier 2011; Hoerling et al. 2013; Mote et al. 2018). Based on Mishra and Lettenmaier (2011), the frequency and magnitude of extreme precipitation events in southwestern US have decreased during the past century. Comparing the period 1959–2008 to 1909–1958, the flood magnitudes have also decreased in the southwest (Peterson et al. 2013). For the twenty-first century, air temperature is projected to continue to increase. Kunkel et al. (2013) reported that if current greenhouse gas (GHG)



emissions continue, the average temperature in the southwest is projected to increase by 3.0–5.3 °C (3.6–4.2 °C in SB) by the end of this century. Even if the GHG emissions are substantially reduced, a temperature increase of 1.9–3.0 °C (1.9–2.5 °C in SB) is still expected. Under this warmer environment, streamflow dynamics are likely to be impacted by changes in precipitation characteristics (e.g., total storm magnitude, peak intensity, and time between storms) and evapotranspiration (Kenneth et al. 2010; Das et al. 2011a; Orlowsky and Seneviratne 2012; Cayan et al. 2013; Johnson et al. 2015; Warner et al. 2015; Feng et al. 2016). Johnson et al. (2015) and Orlowsky and Seneviratne (2012) indicate that the average annual precipitation in the southwest will experience a decline during the twenty-first century. However, Warner et al. (2015) suggest that the mean winter precipitation along the west coast of the USA will increase by 11–18% by the end of this century, with the frequency of daily precipitation extremes increasing by up to 290% under RCP 8.5. Impacted by altered precipitation patterns and increased air temperature, flood magnitudes are likely to increase and larger-than-historical floods are likely by the end of the twenty-first century (Das et al. 2011b).

Much of the previous research on climate change and the resulting impacts on streamflow regimes in the southwestern US focused on inland regions like the Colorado River Basin and Sierra Nevada watersheds (Das et al. 2011a; Vano et al. 2014). Few studies have investigated climate change impacts on streamflow in coastal regions where rainfall is the dominant form of precipitation (Beighley et al. 2003). Johnson et al. (2015) suggested that annual river discharge from coastal watersheds along the western US will change slightly by the mid-twenty-first century but that high flows may increase by 10-20% based on six climate change scenarios from the North American Regional Climate Change Assessment Program. However, Burke and Ficklin (2017) suggest that the projected peak streamflow will likely decrease and occur later in the season along coastal southern California in late-twenty-first century under RCP 8.5. To better understand the potential impacts of future climate conditions on streamflow from watersheds draining a portion of coastal California, we performed an analysis to address the following questions: (1) how will the meteorological conditions in SB change under a warming climate; (2) how will the streamflow quantity (both mean and peak flows) be impacted both temporally and spatially; and (3) what are the implications of these hydrometeorological changes for flood control infrastructure and coastal ecosystem in the SB?

2 Data and methods

2.1 Study site

The study region is defined by coastal Santa Barbara County, California, watersheds draining into the Santa Barbara Channel from just west of the Ventura River to just east of Point Conception (Fig. 1). The combined land area is roughly 750 km² with 135 watersheds ranging from 0.1 to 123 km². The local climate is Mediterranean, which is characterized by moderately warm, dry summers and cool, moist winters. The average minimum temperature is about 3 °C occurring in January, and the average maximum temperature is 25 °C occurring in August based on monthly data for the period 1915–2011 (Livneh et al. 2013). The average annual precipitation is 580 mm for the period 1950–2013 based on gauge-based, re-analysis estimates (Livneh et al. 2015). Most of the annual precipitation occurs in fall/winter with 85% of rainfall occurring in the Nov–Mar period. Based on the 2006 National Land Cover database (Homer



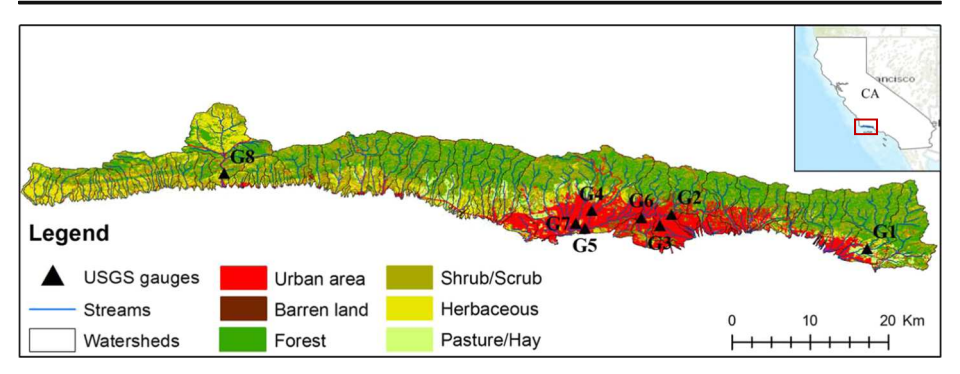


Fig. 1 Watershed boundaries, streamline networks, USGS gauge locations for the study region; numbers next gauge symbols indicate their site IDs listed in Table S1. The plot at top right of the figure indicates the location of Santa Barbara and fringing watersheds

et al. 2015), the dominant land cover categories are forests (34%), shrubs (31%), urban (18%), and herbaceous (13%).

2.2 Data

Daily streamflow data obtained from eight USGS gauge records (Fig. 1; Table S1), gridded observations of daily precipitation (total) and temperature (minimum, maximum and mean) with a spatial resolution of 0.0625°×0.0625° (roughly 6 by 6 km) for the period 1950–2013 (Livneh et al. 2015) are used to calibrate and validate the hydrologic model. For the historical (1961-2000) and future climate simulations (2021-2100), downscaled precipitation and temperature (Pierce et al. 2014; Pierce et al. 2015) from ten climate models (Table 1) in Coupled Model Inter-Comparison Project, Phase 5, (CMIP5) (Taylor et al. 2012) for two emission scenarios RCP 4.5 and RCP 8.5 (Moss et al. 2010) are used. RCP 4.5 describes a stabilization pathway in which the radiative forcing is stabilized at 4.5 w/m² after 2100, while RCP 8.5 is an increasing pathway where the radiative forcing reaches > 8.5 w/m² by 2100 and continues to rise. The GCMs are selected based on their performance in representing historical climate dynamics at global, southwest US and CA state scales (Pierce et al. 2018). The National Land Cover Database (NLCD) for 2006 (Homer et al. 2015) is used to quantify the land cover distribution throughout the study region. The Global Soil Dataset for use in Earth system models (GSDE) is used to estimate saturated hydraulic conductivity and saturated moisture content. To determine net radiation for estimating potential evapotranspiration (PET), the 16-day composite albedo product (MCD43C3) with a spatial resolution of 0.05°× 0.05° and the monthly aerosol optical depth product (MOD08M3) with a spatial resolution of 1.0° × 1.0° both derived from NASA's Moderate Resolution Imaging Spectroradiometer (MODIS) onboard the Terra and Aqua satellites, are used.

2.3 Hydrologic modeling

The Hillslope River Routing (HRR) model (Beighley et al. 2009) is used to simulate streamflow. The HRR model utilizes an irregular computational grid and parallel computing to simulate: (a) vertical water and energy balance through vegetation and soil layers; (b) lateral hydraulic transport from upland areas; and (c) channel hydraulics. The kinematic approximation is used for simulating surface and subsurface runoff from hillslopes to channels; and



Table 1 Relative changes (%) in P, PET, $Q_{\rm m}$, and $Q_{\rm p}$ over the study region for future conditions as compared to historical period derived from P and T predictions from 10 downscaled GCMs for emission scenario RCP 8.5; the results are area-averaged from the 135 watersheds draining the study region; italic numbers indicate significant changes at 0.10 significance level based on Mann-Whitney U test

GCM ID	CMIP5 Model Acronyms	Historical 1961–2000				Future (RCP 8.5)								
						2021–2060				2061–2100				
		P (mm)	PET (mm)	Q _m (mm)	Q _p (cfs)	P (%)	PET (%)	Q _m (%)	Q _p (%)	P (%)	PET (%)	Q _m (%)	Q _p (%)	
1	ACCESS1-0	614	1306	113	4942	-9.7	5.3	0.4	-9.3	-7.8	10.2	0.8	10.6	
2	CanESM2	605	1312	108	4376	8.2	5.7	51.9	58.6	50.5	10.9	256.6	207.8	
3	CCSM4	615	1311	109	4338	-6.1	4.1	-1.2	14.0	2.1	6.3	30.3	60.9	
4	CESM1-BGC	587	1313	109	4596	12.0	3.2	20.5	20.9	33.6	6.0	99.4	106.3	
5	CMCC-CMS	573	1318	96	4084	-12.7	3.5	-36.4	8.7	-12.3	8.2	-34.2	-8.0	
6	CNRM-CM5	620	1309	106	4229	14.0	3.9	66.3	59.6	13.4	8.4	71.9	69.6	
7	GFDL-CM3	597	1303	95	3798	-4.2	7.1	-1.7	7.4	0.4	13.7	26.3	43.3	
8	HadGEM2-CC	602	1305	98	4178	-8.1	5.0	-13.8	-3.0	0.1	10.6	58.7	103.3	
9	HadGEM2-ES	606	1310	97	4293	-0.4	5.3	32.6	24.5	0.4	8.3	44.0	78.3	
10	MIROC5	574	1309	125	4518	-6.1	4.8	-20.8	0.4	-21.0	6.1	-41.8	-34.7	

diffusion wave routing is used for channel flow. Here, PET is estimated using the Priestley and Taylor method (Priestley and Taylor 1972) with the Food and Agriculture Organization of the United Nations (FAO) limited climate data approximations (Raoufi and Beighley 2017). To generate surface runoff in the HRR model, a runoff coefficient approach is used. It assumes that runoff at time t, is $C \times P_b$, where C is the runoff coefficient, which varies based on land cover and soil moisture, and P_t is the precipitation rate at time t. Here, two runoff coefficients (initial and final) are used for each model unit, with a soil moisture threshold (θ_x) to switch between the two coefficients. The three parameters are determined based on calibration and distributed to un-gauged locations based on land cover characteristics. A Monte Carlo-based calibration procedure was implemented to estimate the optimal model parameters. Based on the availability of streamflow data, the calibration period was 1984–2013. The HRR model is forced with gridded precipitation and temperature estimates derived from gauged observations (Livneh et al. 2015). USGS streamflow measurements from fvie of the eight gauges are used for calibration; the remaining three gauges are used for validation. For the days with missing streamflow, interpolation was used to estimate flow values based on relationships between flow values at the gauge with missing data and its neighboring gauge. Here, only five gauges are used for calibration and three gauges for validation due to (1) a very short period of overlapping observations when considering all eight gauges (i.e., less than 3 years from 1983/10/28 to 1986/9/30 as shown in Table S1) that increases substantially (1983/10/28current) when considering only five gauges; (2) that some of the calibrated model parameters are watershed-specific (e.g., the wet runoff coefficient is a function of the urban area fraction, which varies from watershed to watershed, details discussed later) and validation at gauges not used for calibration can assess if the established relationships (such as the linear relationships between wet runoff coefficient and urban area fraction) are valid; and (3) that the three validation gauges provide streamflow records of a time period that is different from the calibration period (Table S1). Thus, splitting the gauges into five calibration and three validation gauges provides assessment for model performance for both spatial and temporal variabilities.

The parameters included in the calibration influence lateral and vertical transport and surface runoff generation processes: k_s (coefficient to adjust surface roughness), k_v (coefficient to adjust vertical hydraulic conductivity), θ_x (threshold in soil moisture separating dry and wet runoff conditions), C_1 (runoff coefficient for $\theta < \theta_x$), and C_2 (runoff coefficient for $\theta \ge \theta_x$). The parameter ranges are defined based on the hydrologic characteristics of the study region and previous modeling experience (Beighley and Moglen 2002; Beighley et al. 2005; Beighley et al. 2008). The performance metrics used for optimal parameter identification are bias (to assess water balance, bias) and annual peak error (to assess flooding conditions, e_D).

For calibration, thousands of parameter sets are randomly selected from predefined parameter spaces (Table S2). Next, the HRR model is implemented for the calibration period using each parameter set, and the best parameter set for each gauged-watershed based on minimum error (*e*) at each gauge location is selected:

$$e = \sqrt{\overline{bias}^2 + \overline{e_p}^2} \tag{1}$$

where \overline{bias} and $\overline{e_p}$ are mean bias (%) and mean peak error (%), respectively, based on averaging annual values over the entire calibration period. To estimate the model parameters at non-calibrated watersheds, the optimal values from each gauge are then related to upstream



watershed characteristics (e.g., land cover features). For example, $C_2 = m_2 \ U + b_2$, where m_2 and b_2 are linear regression coefficients determined by relating the optimal C_2 coefficients and percent urban land cover (U) for each gauged-watershed. For those which are not significantly correlated with any hydrogeologic characteristics, their values are estimated when the overall cost function (e' in Eq.2) is minimized. Next, to refine the values of the regression coefficients (e.g., m_2 , b_2), a second calibration step was performed, during which these coefficients were randomly selected with other parameters (which are not significantly correlated with watershed characteristics) locked as the optimal values obtained from the first calibration step. Then, the HRR model is again implemented for all parameter sets and the optimal parameter set is selected based on the minimum mean performance metric (e'):

$$e' = \frac{1}{n} \sum_{i=1}^{i=n} e_i \tag{2}$$

where e' is the mean error from all calibrated watersheds; e_i is the error calculated using Eq. 1 at the *i*th watershed; and n is the number of calibrated watersheds (i.e., 5 in this study). In this second iteration, the mean performance metric from all gauges (Eq. 2) is used because relevant parameters are now varied based on local catchment characteristics (e.g., land cover fractions). The parameters' definition, ranges, and final values are shown in Supplemental Table S2.

2.4 Statistical analysis

To test if simulated future precipitation (P), PET, mean annual streamflow $(Q_{\rm m})$, and annual peak flows $(Q_{\rm p})$ are significantly different from those for the historical period, the Mann-Whitney U test is applied. Mann-Whitney U test is a non-parametric method for testing if two samples are selected from the same population. The historical period (i.e., 1961-2000) was used as the comparison base to investigate possible changes in two future projection periods having the same duration: 2021-2060 and 2061-2100. The null hypothesis of Mann-Whitney U test is that the difference in the mean between the two samples is equal to 0. In this work, we use 0.10 as the significance level to test the hypothesis. The Mann-Whitney tests were performed on both annual and seasonal series.

2.5 Definitions specific to this study

Seasons are defined as winter (JFM), spring (AMJ), fall (OND), and summer (JAS). To investigate potential changes in the duration of the rainy season, the accumulated P series in each water year was determined, and the number of days between the 10 and 90% of the accumulated P series was defined as the duration of the rainy season (i.e., number of days accounting for 80% annual P). Though this definition is subjective, it provides a quantitative metric that can be determined for all years. To obtain the integrated precipitation over a watershed, the hydrologic model was simulated assuming 100% of the precipitation is transferred to surface runoff with no other losses and routed to the watershed outlet providing hydrographs that represent the cumulative event precipitation volumes. Here, the groundwater or baseflow was assumed to be zero in this simulation. In this region, baseflow is a small fraction of streamflow (Beighley et al. 2003), which makes it reasonable to estimate precipitation dynamics by transferring 100% precipitation to surface runoff. To determine the number of rainfall events, we count the number of 100% rainfall-derived hydrograph peaks for which there are no other higher peaks within five consecutive days.



3 Results

3.1 Calibration results

In this study, K_s , K_v , and C_1 were not found to be significantly correlated with any characteristics of the watersheds. Thus, these parameters are assumed to be uniform for all model units; C_2 and θ_x were found to be linearly related with the urban area fraction of the gauged watersheds, that is, $C_2 = m_2 \ U + b_2$ and $\theta_x = m_\theta U + b_\theta$ (definitions can be found in Table S2), and the regression coefficients (i.e., m_2 , b_2 , m_θ , and b_θ) were calibrated in the second step. The final values of calibrated parameters are shown in Table S2.

The final error measures of the calibrated model and the resulting streamflow hydrographs and probability distributions at each gauge compared to USGS streamflow measurements are shown in Supplemental Table S3 and Fig. S1. The calibrated model performs well for representing both baseflow and peak magnitudes and timing. At calibration gauges, the bias errors vary between -11.2 and +9.4% and the peak errors are within $\pm 15\%$ except for gauge 11120000 where the bias in precipitation data results in lower simulated peaks (-25.7%) than gauge records. At validation gauges, the model bias ranges from -29.1 to 2.6%, and the peak errors vary between -24.5 and -9.1% except for gauge 11120550. From Fig. S1, we can find the calibrated model performs good at representing baseflow and peak flow dynamics as well as the probability distribution characteristics at all gauges.

3.2 Changes in P, PET, $Q_{\rm m}$, and $Q_{\rm p}$ area-averaged over the entire study region

Relative changes in the hydro-meteorological variables (P, PET, $Q_{\rm m}$, and $Q_{\rm p}$) in the future, based on projections from 10 GCMs under RCP 8.5, are summarized in Table 1. For space conservation, only results under RCP 8.5 are shown here, and the results for RCP 4.5 can be found in Supplementary material (Table S4).

For 2021-2060, 7 out of 10 models show a decrease in annual P ranging from -0.4 to -12.7%, while the other three models show an increase in P ranging from 8.2 to 14%. However, none of these changes are statistically significant. In contrast, all ten models show a significant increase in PET for 2021–2060. The increase varies from 3.2 to 7.1%. Half of the models show an increase in $Q_{\rm m}$, while the other half show a decrease in $Q_{\rm m}$. The changes in $Q_{\rm m}$ are consistent with those in P (i.e., increase or decrease in both P and $Q_{\rm m}$) for most of the models (except for M1 and M9), suggesting the variability in annual precipitation is the primary factor controlling variations in streamflow quantities. Compared to $Q_{\rm m}$, changes in Qp are less consistent with those in P. For half of the models, changes in Qp are opposite to changes in P (e.g., increase in Qp vs. decrease in P, and vice versa), which implies that altered annual precipitation is not sufficient to explains variations in streamflow dynamics (e.g., maximum daily discharge). During this period, changes in all variables, except PET, are not statistically significant (Table 1). During 2061–2100, more models show increase than decrease in all four variables. Three models show statistically significant increases in both $Q_{\rm m}$ and $Q_{\rm p}$; however, no models show a significant decrease in any of these quantities. In addition, the magnitudes of changes in all four variables are higher during 2061–2100, as compared to the period 2021– 2060. The higher magnitude of changes in the second half century is consistent with the emission pathway in which GHG continues to increase till 2100.

Under RCP 4.5, the patterns of changes are similar for all variables except for precipitation (Table 1 and Table S4). During 2021–2060, more models show an increase in *P* under RCP 4.5



(5/10 for RCP 4.5 and 3/10 for RCP 8.5), and more models show significant changes in P (and subsequently in $Q_{\rm m}$ and $Q_{\rm p}$) under RCP 4.5 (2 significant increase and 1 significant decrease under RCP 4.5, and none under RCP 8.5). In contrast, during 2061–2100, less models show an increase in P under RCP 4.5 (4/10 for RCP 4.5 and 7/10 for RCP 8.5) and less significant changes in $Q_{\rm m}$ and $Q_{\rm p}$. This suggests that, under higher emission scenario RCP 8.5, the changes in hydro-meteorological variables are more obvious (i.e., dominant change shift from decrease to increase).

3.3 Spatial variations in changes in P, $Q_{\rm m}$, and $Q_{\rm p}$

The relative changes in P, $Q_{\rm m}$, and $Q_{\rm p}$ for each individual watershed under future climate conditions (2061–2100) projected by 10 GCMs under RCP 8.5 are shown in Fig. 2. The detailed results for 2021-2060 under RCP 8.5 and for both periods under RCP 4.5 can be found in Supplementary Material (Figs. S2-S4 and Tables S5-S8). The results for the two emission scenarios are similar, but the magnitudes of the changes in Q_m and Q_p are higher under RCP 8.5, especially during the second half of twenty-first century. From Fig. 2, we find that the median value of changes in P over each watershed is close to zero (within $\pm 2\%$) under RCP 8.5. However, the median changes in both $Q_{\rm m}$ and $Q_{\rm p}$ are positive (+29% to +58% for $Q_{\rm m}$ and +51% to +99% for $Q_{\rm p}$) and much large than those for P. Although the variability (or uncertainty) of relative changes in P and PET (not shown in Fig. 2) among models is almost uniformly distributed throughout the study region, the variability of relative changes in Q_m and $Q_{\rm p}$ among models tends to shrink from west to east, especially for $Q_{\rm p}$. In the western region, most of the watersheds are moderately steep mountains covered by forested and shrub lands. In the middle and eastern region, watersheds contain steep, forested mountains with less steep coastal plains containing urban and agricultural development (Beighley and Moglen 2002; Beighley et al. 2005; Beighley et al. 2008). In the watersheds where the mountains are forested and moderately steep with little development, runoff generation is nonlinear and sensitive to rainfall rates and the duration of time between events. However, in the steep mountains and urban areas, runoff generation is more consistent and controlled largely by alterations in P magnitudes. Therefore, in the west, the nonlinearity of hydrologic response to P is amplified. For example, when soil moisture is near the point of runoff production, a slight increase in P can result in a disproportionately large increase in Q. This may explain the large variability in $Q_{\rm p}$ changes among models in the western region as compared to the middle and eastern regions. In addition, from west to east, the soil composition has less silt and more sand fractions. Thus, the soils in the western watersheds tend to have lower porosity as compared to the soils in the eastern watersheds, which can also increase runoff when the rainfall is intensified.

3.4 Seasonality

As discussed in Section 3.3, the analysis of relative changes in P, $Q_{\rm m}$, and $Q_{\rm p}$ for future climate projections reveals changes in streamflow characteristics that might not have been anticipated for a system in which the median change in annual precipitation from the model ensemble is only $\pm 2\%$. For example, as shown in Fig. 2, annual streamflow increases by up to 58% and annual peak flows increase by 99% during 2061–2100 under RCP 8.5 based on the ensemble medians; however, the median change in annual P is less than 2%. The nonlinear response of changes in streamflow to alterations in precipitation



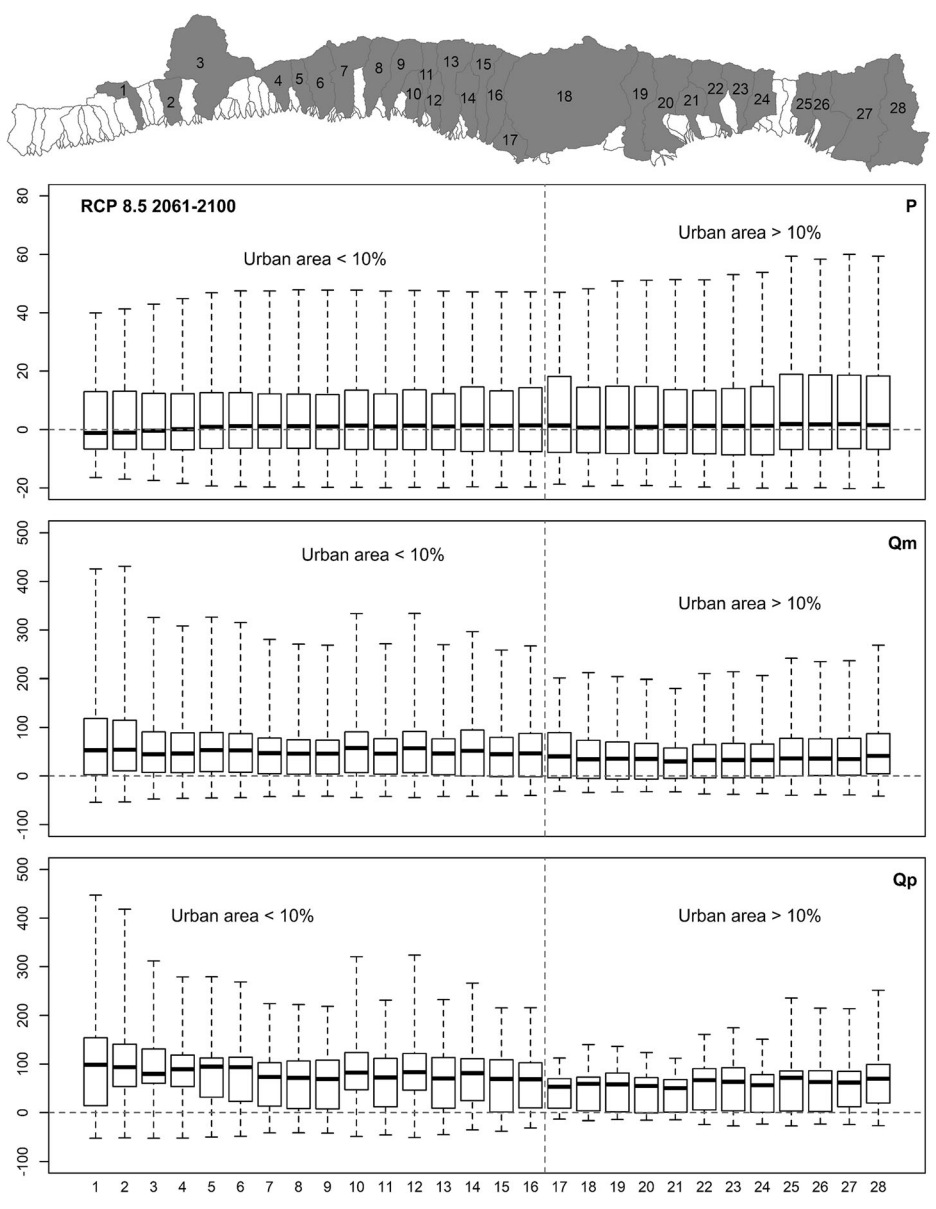


Fig. 2 Relative changes (%) of annual precipitation, annual streamflow, and annual peak flow in the major SB watersheds (indicated by the gray watersheds in the map) during 2061–2100 based on 10 GCM output simulations for scenario RCP 8.5; each bar depicts relative changes in minimum, maximum, median, 1st and 3rd quartiles for the ensemble outputs; bars from left to right spatially corresponding to watersheds from west to east. For clarity, only watersheds with drainage areas larger than 7 km², which account for roughly 83% of the study area, are shown

amount may result from two possible mechanisms: (1) the grouping of smaller rainfall events closer together leading to more rainfall occurring on wetter soils or (2) the magnitudes of the few larger rainfall events increasing. To evaluate the likely process,



Table 2 Relative change (%) in the number of rainfall events for the future conditions as compared to historical period (1961–2000) derived from *P* predictions from 10 downscaled GCMs for emission scenario RCP 8.5

GCMID	1961–2000				2021–2060	(%)			2061–2100 (%)				
	<18 mm/ day	18–36 mm/ day	> 36 mm/ day	All events	< 18 mm/ day	18–36 mm/ day	> 36 mm/ day	All events	< 18 mm/ day	18–36 mm/ day	> 36 mm/ day	All events	
1	8	2	1	12	- 13.5	-12.6	- 12.7	-13.2	-23.1	-6.5	6.8	-17.3	
2	8	2	1	11	-5.1	1.4	20.9	-1.6	-6.2	-9.0	107.3	3.6	
3	8	2	1	12	-12.0	-14.6	-9.3	-12.2	-16.6	-13.2	14.0	-13.0	
4	9	2	1	12	-13.2	16.2	32.4	-4.6	-12.8	20.1	81.1	0.3	
5	9	2	1	11	4.2	-21.8	1.5	-0.4	-14.7	-6.3	3.5	-11.9	
6	9	2	1	12	-8.7	5.4	33.0	-2.4	-18.9	-10.4	36.9	-12.4	
7	9	2	1	12	-11.3	-13.0	11.7	-9.9	-23.3	0.7	35.6	-14.5	
8	8	2	1	11	-2.2	-4.2	-2.7	-2.6	-16.1	-23.9	20.8	-14.2	
9	9	2	1	12	-9.5	-9.4	17.3	-7.1	-27.6	-29.9	37.7	-22.2	
10	8	2	1	11	-3.4	-15.1	16.1	-3.9	- 19.9	-24.8	-4.7	-19.5	

further analyses on the frequency and magnitudes of rainfall events were performed and the results are shown in Table 2. Almost all models show that the number of rainfall events will decrease during twenty-first century (in median, roughly -6% and -12% for 2021-2060 and 2061–2100, respectively) under RCP 8.5, but the decrease is not uniform with respect to rainfall intensities (Table 2). The number of rainfall events with low (< 18 mm/ day) to moderate (18–36 mm/day) intensities decreases (in median, -7.5% for low events and -6.8% for moderate events during 2021-2060; -17.9% and -10.3% during 2061-2100), while the number of large rainfall events (> 36 mm/day) increases (12.3% during 2021–2060 and 33.9% during 2061–2100). These results suggest that it is the increase in rainfall magnitudes and frequency of the larger storms that leads to the increase in annual $Q_{\rm p}$. For example, for 2021–2060 under RCP 8.5, the frequency of small to moderate rainfall events is likely to decrease by about 8% (ensemble median) contributing to the slight decrease (about 5%) in annual P (as shown in Table 1), while the intensity and frequency of large storms is likely to increase by 2 and 15%, respectively, which results in an increase in annual Q_p (Tables 1–2). For 2061–2100, the increase in the frequency and magnitude of large rainfall events offsets the decrease in low/moderate P events leading to only a slight increase in annual P but a more evident increase in annual Q_p (Tables 1–2).

The analysis on changes in seasonal precipitation was also performed and the results show an increase in winter precipitation and a decrease in spring and fall during the twenty-first century, which is consistent with findings in a recent study by Swain et al. (2018) which suggest wet season rainfall will shift from marginal (September–October, April–May) to the core rainy season (November–March). Although there is an increase in summer *P*, the increase is defined based on percent change in *P* but provides essentially no difference in streamflow because the magnitude of change is very small. These changes in seasonal precipitation lead to a shift in the timing of seasonality (Fig. 3). The duration of the wet season during the historical period (1961–2000) is 124 days; however, the wet season length is shorter by 11 days and 18 days during 2061–2100, for RCP 4.5 and RCP 8.5, respectively. The detailed wet season lengths projected by 10 models are shown in Table S10. The lengths for 1961–2000 among models vary between 115 and 129 days

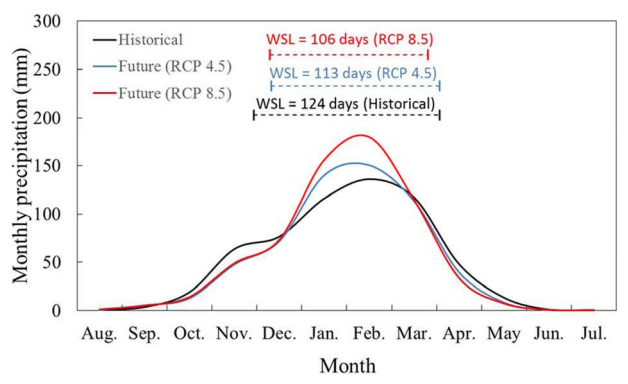


Fig. 3 Monthly precipitation throughout the whole SB coastal basin during historical (1961–2000) and future (2061–2100) periods under both emission scenarios (RCP 4.5 and RCP 8.5). For the future scenario, the median values of monthly precipitation from 10 downscaled GCM projections are used. The dash lines indicate the average period of wet seasons which is defined as the period during which 80% annual precipitation is accumulated (starting from the day when 10% of annual precipitation is accumulated and ending at the day when 90% of annual precipitation is accumulated). WSL stands for wet season length



among models (Table S10). Eight of the 10 models show a shorter rainy season duration, with decreases of 9–23 days (roughly 7–18%) during 2021–2060 under RCP 8.5; all of the models suggest a shorter wet season by 5–28 days (roughly 4–23%) during 2061–2100. The shortening of wet season is mainly due to a late onset of consistent rainfall. The shorter rainy season and more frequent large storms imply that more (and/or larger) storms occur in a shorter period of time, which can lead to wetter initial conditions and more runoff.

For both RCP 4.5 and RCP 8.5, most of the models produce decreased streamflow in spring and fall and increased streamflow in winter (Table 3 and Table S11). However, the magnitude of the increase in winter streamflow is larger than the magnitude of decreases in fall and spring which explains the overall net increase in $Q_{\rm m}$. The change in summer streamflow is negligible considering the usual lack of flow reaching the coast in summer. Given the peak flows typically occur in the winter period, the increase in winter streamflow also leads to the increase in $Q_{\rm p}$. Eight of the 10 models show an increase in $Q_{\rm p}$ during 2061–2100 under RCP 8.5 for which the changes are statistically significant from four models (Table 3). As shown in Table 3, the patterns of changes in seasonal streamflow are consistent during twenty-first century under RCP 8.5 that is, both periods (2021–2060 and 2061–2100) show decreases in spring and fall streamflow and increase in winter streamflow. However, the statistical significance of the changes is more evident in the latter period, for example, there are four models showing significant increase in Q_p for 2061–2100 compared to only 1 for 2021–2060. In contrast, under RCP 4.5, the statistical significance is more evident for 2021–2060 than 2061–2100, especially for spring and summer, but the direction of changes is similar to that for RCP 8.5 (i.e., decrease in spring and fall streamflow, and increase in winter streamflow), especially for the 2061–2100.

4 Discussion and conclusions

In this study, we find that for coastal southern California watersheds, future climate conditions produce more frequent, larger precipitation events occurring in a shorter rainy season with only a small change in annual precipitation. The enhanced precipitation extremes concentrated in a shorter period leads to more runoff and larger annual peak flows. The nonlinear hydrologic response to altered precipitation series is especially challenging when predicting changes in flood discharges based on projected precipitation. Combined changes in precipitation frequency and magnitude distributions make a noticeable difference on streamflow characteristics. While annual P is a key determinant of annual $Q_{\rm m}$, especially in urban areas, the variability of rainfall event spacings and magnitudes plays a significant role in controlling changes in the annual Q_p. These changes are further amplified in the flood frequency analysis. When using commonly used flood frequency analysis methods (e.g., Log-Pearson type III method, LPIII) to estimate flood frequency distributions for the future climate conditions, the magnitude of a specific return period flood is a function of the moments of the annual Q_p series. Therefore, changes in any of the statistics for the Q_p series may lead to the changes in the estimated flood magnitudes. For example, as shown in Fig. 4, during 2061-2100 under RCP 8.5, the median increase among the 10 models is 43% for annual $Q_{\rm m}$, 76% for $Q_{\rm p}$ and 101% for the 100-year discharge. These changes are especially important when we consider that the average change of annual precipitation is only 2%. Thus, changes in the magnitude and variability (inter- and intra-



Table 3 Relative changes (%) in seasonal streamflow over the study region for the future conditions as compared to historical period (1961–2000) derived from P and T predictions from 10 downscaled GCMs for emission scenario RCP 8.5; italic numbers indicate significant changes at 0.10 significance level based on Mann-Whitney U test

GCM ID	Historical				Future (RCP 8.5)								
	1961–2000		2021–2060				2061–2100						
	Spring (mm)	Summer (mm)	Fall (mm)	Winter (mm)	Spring (%)	Summer (%)	Fall (%)	Winter (%)	Spring (%)	Summer (%)	Fall (%)	Winter (%)	
1	12.0	0.1	1.6	100.8	-61.0	14.7	- 37.6	9.8	- 69.8	62.1	- 45.1	8.7	
2	8.0	0.1	3.1	99.5	-6.8	-0.4	179.6	53.0	-35.1	1.3	77.5	276.4	
3	7.4	0.1	3.8	96.4	- 79.4	-1.4	-24.8	9.9	-57.3	-0.8	-66.4	42.8	
4	6.3	0.1	6.6	96.4	35.5	119.2	-66.9	27.9	94.7	1.4	-72.2	110.3	
5	7.7	0.1	4.3	72.8	- 63.5	-0.2	- 54.6	-20.4	- 77.8	38.7	-14.9	-20.5	
6	6.8	0.1	4.0	91.1	-49.4	0.6	80.9	82.4	-15.0	78.3	-17.5	89.4	
7	6.8	0.1	3.6	79.0	-4.6	0.1	-40.3	7.0	-6.8	0.4	6.3	39.4	
8	10.1	0.1	5.2	84.9	-52.5	-0.2	-53.8	-6.8	30.9	142.1	- 46.2	63.8	
9	8.3	0.1	2.5	88.9	25.8	1.3	8.8	33.8	-71.2	-0.2	115.8	48.8	
10	7.2	0.1	0.9	110.5	-66.9	-0.4	222.2	-12.9	-32.1	-0.5	9.5	-39.5	

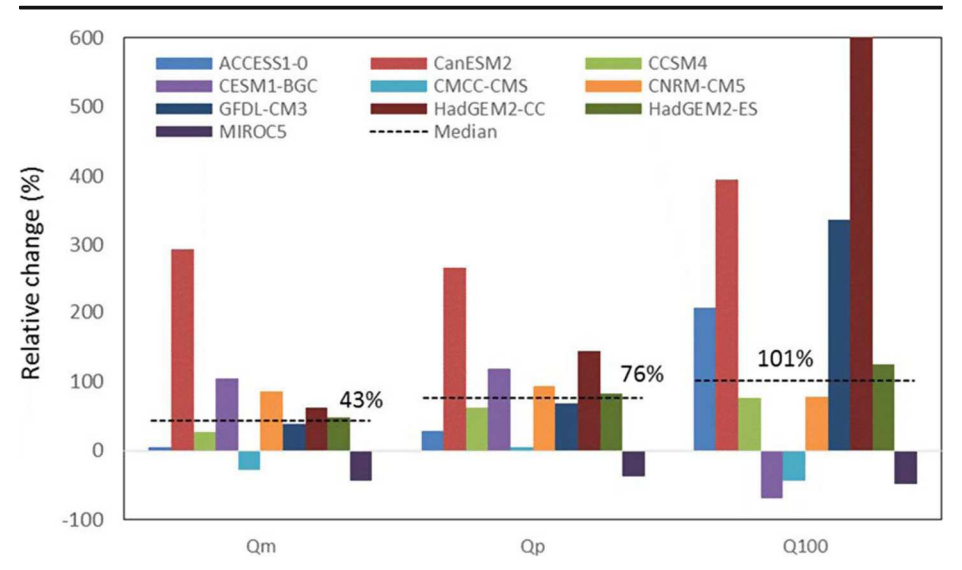


Fig. 4 Relative changes of annual streamflow $(Q_{\rm m})$, peak flow $(Q_{\rm p})$ and 100-year flood discharge (Q_{100}) averaged over the major SB watersheds (same as in Fig. 3) during 2061–2100 based on each model projection under emission scenario RCP 8.5. Black dash lines are the median values among 10 models, and they are 43%, 76%, and 101% for $Q_{\rm m}$, $Q_{\rm p}$ and Q_{100} , respectively

annual) of P as well as spatial variations in land cover and soil properties can lead to disproportionate changes in estimated flood discharges and should be taken into consideration when designing civil infrastructure and managing water resource.

The changes in discharge and seasonality will also impact the export of nutrients and sediment to the coastal ecosystem. The fluxes of nutrients (e.g., nitrate, phosphate and ammonium) and sediment (e.g., total suspended sediment) from SB watersheds are significantly and positively associated with hydrologic variability (Aguilera and Melack 2018). This may imply that the nutrients/sediment export to the coastal ecosystem will likely increase due to the increase in both the magnitudes and frequency of high discharge events. Nutrients and sediments build up in dry season and progressively flushing in wet season (Bende-Michl et al. 2013; Lewis and Grimm 2007; Aguilera and Melack 2018). The majority of nutrients/sediment fluxes occurs at the beginning of wet season (Homyak et al. 2014). Therefore, the shift in seasonality (a later onset of wet season) can result in changes in the timing of nutrients/sediment export to the coastal zone. The lengthening of dry season, decreased streamflow in dry season as well as increased temperatures in the future, will likely make the SB region more vulnerable to wildfires, which will also elevate the nutrients/sediment export to the coastal aquatic environment (Aguilera and Melack 2018). Therefore, the findings in this study imply that the nutrients/sediment export to the coastal ecosystem will likely increase in the future and that the seasonal variation in these fluxes may also be impacted, which will subsequently impact aquatic environment in the coastal ecosystem.

As an integration of water stores and fluxes in the land-ocean-atmosphere, the hydrologic cycle can be impacted by climate change in various ways. Climate change may impact streamflow by temperature increases or through changes in the hydrometeorological variables. In arctic and boreal/snow-dominant regions (like Europe and northern US), the increase in temperature can lead to a shift of precipitation forms and



timing of runoff, and thus altering streamflow seasonality (Barnett et al. 2005; Barnett et al. 2008; Schneider et al. 2013; Gelfan et al. 2017). In monsoonal regions (e.g., China), streamflow will likely increase especially during high-flow season, mainly due to the intensified northern hemisphere summer monsoon (Eisner et al. 2017). In areas strongly impacted by atmospheric river (AR) events, such as western US and southwestern South America, streamflow especially the extremes will be likely affected by the intensified AR activities under a warmer climate (Vicky et al. 2018). The findings in this study provide a compliment to existing studies regarding climate change impacts on hydrology. The results in this study suggest that, in the rain-dominant region like coastal SB with a Mediterranean/semi-arid climate, the future climate conditions will likely lead to a later onset and intensified wet season streamflow mainly due to the changes in precipitation patterns. These findings are consistent with previous studies (e.g., Schneider et al. 2013; Mote et al. 2018; Burke and Ficklin 2017) in terms of changes in seasonality in Mediterranean climate regions. Although the study is focused on a specific and relatively small region, it provides a framework for assessing the hydrologic impacts of future climate conditions in other regions. As highlighted here, changes in annual precipitation do not tell the whole story. Regions, especially semi-arid or Mediterranean regions, where rainfall is often limited and rainfall-runoff response is highly nonlinear, may see large changes in runoff and peak streamflow with relatively small changes in precipitation.

In this study, the hydrologic model parameters were calibrated using short periods (e.g., 1984 to 2013) of historical streamflow observations and are assumed to be temporally constant (i.e., parameters not changing to reflect potential changes in land use/land cover or changes in hydrologic responses resulting from the altered climate conditions). However, under a changing climate, the streamflow dynamics can be non-stationary, which suggests the calibrated model which performs well in representing historical streamflow dynamics may not work well for future scenarios. As such, the simulation results in this work may be biased due to using stationary model parameters. However, the conclusion that future streamflow (especially extremes like annual peak flow and 100-year flood discharge) will increase is likely valid considering urbanization tends to result in quicker and/or higher peak discharges. Parameter equifinality (i.e., multiple parameter sets meet similar cost function criteria) can be another issue. In this study, only one optimal parameter set was selected for future simulation. Further work on parameter equifinality will be performed to address its effect on simulated streamflow and the associated uncertainties. In addition, land cover/land use change and other potential anthropogenic activities are not integrated into the simulation for future streamflow. For example, SB may change zoning policies or expand/alter their stormwater/flood infrastructures in the future to mitigate future impacts. Building on this effort, if information on projected land cover change and/or anthropogenic activities can be estimated, it can be integrated into this modeling framework to optimize potential mitigation strategies.

In general, the results in this study show that climate changes may alter the seasonal pattern of precipitation in coastal Santa Barbara during the twenty-first century, that is, more frequent large storms concentrated in a shorter wet season as compared to the historical period 1961–2000. This alteration may yield a pronounced increase in the streamflow, especially the low-frequency flows, even though mean annual precipitation is likely to change by only a small fraction. The nonlinear hydrologic response to altered precipitation patterns may result in large increases in estimated large floods, which is especially important for the design and



management of civil infrastructure and water resources. The changes in hydrologic variabilities and seasonality will also impact nutrient/sediment export to the coast and subsequently affect the aquatic environment in the coastal ecosystem.

Acknowledgements We thank Dr. David Pierce for the climate model downscaling datasets, support for which was provided by the California Energy Commission (CEC-500-10-041) and the US Geological Survey through the Southwest Climate Science Center and from NOAA through the California Nevada Climate Applications Project (CNAP) Regional Integrated Science Applications (RISA) program.

Author contribution D.F., E.B., J.M. and D.C. designed the framework of this study. D.F. and E.B. wrote the paper with support from J.M. R.R. developed PET data, Y.Z. contributed to the HRR model setup, S.I. performed the precipitation and temperature downscaling. D.F. performed the model calibration, future simulations, and results analyses.

Funding information This research was supported by the Santa Barbara Area Coastal Ecosystem Vulnerability Assessment (SBA CEVA) with funding from the NOAA Climate Program Office Coastal and Ocean Climate Applications (COCA) and Sea Grant Community Climate Adaptation Initiative (CCAI), NASA's Terrestrial Hydrology (NNX12AQ36G, NNX14AD82G) and SWOT (NNX16AQ39G) Programs, and the National Science Foundation's Long-Term Ecological Research (LTER) program (Santa Barbara Coastal LTER—OCE9982105, OCE-0620276, and OCE-123277).

Compliance with ethical standards

Conflict of interest The authors declare that they have no competing interests.

Publisher's note Springer Nature remains neutral with regard to jurisdictional claims in published maps and institutional affiliations.

References

- Aguilera R, Melack JM (2018) Relationships among nutrient and sediment fluxes, hydrological variability, fire and land cover in coastal California catchments. Biogeosciences, Journal of Geophysical Research
- Barnett TP, Adam JC, Lettenmaier DP (2005) Potential impacts of a warming climate on water availability in snow-dominated regions. Nature 438(7066):303–309
- Barnett TP, Pierce DW, Hidalgo HG, Bonfils C, Santer BD, Das T, Bala G, Wood AW, Nozawa T, Mirin AA (2008) Human-induced changes in the hydrology of the western United States. Science 319(5866):1080– 1083
- Beighley R, Moglen G (2002) Trend assessment in rainfall-runoff behavior in urbanizing watersheds. J Hydrol Eng 7(1):27–34. https://doi.org/10.1061/(ASCE)1084-0699(2002)7:1(27)
- Beighley RE, Moglen GE (2003) Adjusting measured peak discharges from an urbanizing watershed to reflect a stationary land use signal. Water Resour Res 39(4):1093. https://doi.org/10.1029/2002WR001846
- Beighley RE, Melack JM, Dunne T (2003) Impacts of California's climatic regimes and coastal land use change on streamflow characteristics. JAWRA J Am Water Res Assoc 39(6):1419–1433. https://doi.org/10.1111/j.1752-1688.2003.tb04428.x
- Beighley RE, Dunne T, Melack JM (2005) Understanding and modeling basin hydrology: interpreting the hydrogeological signature. Hydrol Process 19(7):1333–1353. https://doi.org/10.1002/hyp.5567
- Beighley RE, Dunne T, Melack JM (2008) Impacts of climate variability and land use alterations on frequency distributions of terrestrial runoff loading to coastal waters in Southern California. JAWRA Journal of the American Water Resources Association 44(1):62–74. https://doi.org/10.1111/j.1752-1688.2007.00138.x
- Beighley RE, Eggert KG, Dunne T, He Y, Gummadi V, Verdin KL (2009) Simulating hydrologic and hydraulic processes throughout the Amazon River Basin. Hydrol Process 23(8):1221–1235. https://doi.org/10.1002 /hyp.7252
- Bende-Michl U, Verburg K, Cresswell HP (2013) High-frequency nutrient monitoring to infer seasonal patterns in catchment source availability, mobilisation and delivery. Environ Monit Assess 185(11):9191–9219



- Bonfils C, Santer BD, Pierce DW, Hidalgo HG, Bala G, Das T, Barnett TP, Cayan DR, Doutriaux C, Wood AW (2008) Detection and attribution of temperature changes in the mountainous western United States. J Clim 21(23):6404–6424
- Brown C (2010) The end of reliability. J Water Resour Plan Manag 136(2):143–145. https://doi.org/10.1061/(ASCE)WR.1943-5452.65
- Brzezinski MA, Reed DC, Harrer S, Rassweiler A, Melack JM, Goodridge BM, Dugan JE (2013) Multiple sources and forms of nitrogen sustain year-round kelp growth: on the Inner Continental Shelf of the Santa Barbara Channel. Oceanography 26(3):114–123
- Burke WD, Ficklin DL (2017) Future projections of streamflow magnitude and timing differ across coastal watersheds of the western United States. Int J Climatol 37(13):4493–4508
- Byrnes JE, Reed DC, Cardinale BJ, Cavanaugh KC, Holbrook SJ, Schmitt RJ (2011) Climate-driven increases in storm frequency simplify kelp forest food webs. Glob Chang Biol 17(8):2513–2524. https://doi.org/10.1111/j.1365-2486.2011.02409.x
- Cayan D, Tyree M, Kunkel KE, Castro C, Gershunov A, Barsugli J, Ray AJ, Overpeck J, Anderson M, Russell J et al (2013) Future climate: Projected average. In: Garfin G, Jardine A, Merideth R, Black M, LeRoy S (eds) In assessment of climate change in the southwest United States: A report prepared for the national climate assessment. A report by the Southwest Climate Alliance, Washington, DC, pp 101–125
- Das T, Dettinger MD, Cayan DR, Hidalgo HG (2011a) Potential increase in floods in California's Sierra Nevada under future climate projections. Clim Chang 109:71–94. https://doi.org/10.1007/s10584-011-0298-z
- Das T, Pierce DW, Cayan DR, Vano JA, Lettenmaier DP (2011b) The importance of warm season warming to western U.S. streamflow changes. Geophys Res Lett 38(23):L23403. https://doi.org/10.1029/2011 GL049660
- Eisner S, Flörke M, Chamorro A, Daggupati P, Donnelly C, Huang J, Hundecha Y, Koch H, Kalugin A, Krylenko I, Mishra V (2017) An ensemble analysis of climate change impacts on streamflow seasonality across 11 large river basins. Clim Chang 141(3):401–417
- Feng D, Beighley E, Hughes R, Kimbro D (2016) Spatial and temporal variations in eastern U.S. hydrology: responses to global climate variability. JAWRA J Am Water Resour Assoc 52(5):1089–1108. https://doi. org/10.1111/1752-1688.12445
- Gelfan A, Gustafsson D, Motovilov Y, Arheimer B, Kalugin A, Krylenko I, Lavrenov A (2017) Climate change impact on the water regime of two great Arctic rivers: modeling and uncertainty issues. Clim Chang 141(3): 499–515
- Goodridge BM, Melack JM (2012) Land use control of stream nitrate concentrations in mountainous coastal California watersheds. J Geophys Res Biogeosci 117(G2):G02005
- Hidalgo HG, Das T, Dettinger M, Cayan D, Pierce D, Barnett T, Bala G, Mirin A, Wood A, Bonfils C (2009) Detection and attribution of streamflow timing changes to climate change in the western United States. J Clim 22(13):3838–3855
- Hoerling MP, Dettinger M, Wolter K, Lukas J, Eischeid J, Nemani R, Liebmann B and Kunkel KE (2013). "Present weather and climate: Evolving conditions." In assessment of climate change in the southwest united states: A report prepared for the national climate assessment. A report by the Southwest Climate Alliance. G. Garfin, A. Jardine, R. Merideth, M. Black and S. LeRoy. Washington, DC: 74–100
- Homer CG, Dewitz JA, Yang L, Jin S, Danielson P, Xian G, Coulston J, Herold ND, Wickham JD, Megown K (2015) Completion of the 2011 national land cover database for the conterminous United States-representing a decade of land cover change information. Photogramm Eng Remote Sens 81(5):345–354
- Homyak PM, Sickman JO, Miller AE, Melack JM, Meixner T, Schimel JP (2014) Assessing nitrogen-saturation in a seasonally dry chaparral watershed: limitations of traditional indicators of N-saturation. Ecosystems 17: 1286–1305
- Hossain F, Arnold J, Beighley E, Brown C, Burian S, Chen J, Mitra A, Niyogi D, Pielke R Sr, Tidwell V et al (2015) What do experienced water managers think of water resources of our nation and its management infrastructure? PLoS One 10(11):e0142073. https://doi.org/10.1371/journal.pone.0142073
- Johnson T, Butcher J, Deb D, Faizullabhoy M, Hummel P, Kittle J, McGinnis S, Mearns LO, Nover D, Parker A et al (2015) Modeling streamflow and water quality sensitivity to climate change and urban development in 20 U.S. watersheds. JAWRA J Am Water Resour Assoc 51(5):1321–1341. https://doi.org/10.1111/1752-1688.12308
- Kenneth S, Gary Y, James N, Brent B (2010) Characterizing changes in drought risk for the United States from climate change. Environ Res Lett 5(4):044012
- Kunkel KE, Stevens LE, Stevens SE, Sun L, Janssen E, Wuebbles D, Redmond KT and Dobson JG (2013).
 Regional climate trends and scenarios for the U.S. National Climate Assessment: part 5. Climate of the Southwest U.S. NOAA Technical Report. Washington, D.C., National Oceanic and Atmospheric Administration 87



- Lewis DB, Grimm NB (2007) Hierarchical regulation of nitrogen export from urban catchments: interactions of storms and landscapes. Ecol Appl 17(8):2347–2364
- Livneh B, Rosenberg EA, Lin C, Nijssen B, Mishra V, Andreadis KM, Maurer EP, Lettenmaier DP (2013) A long-term hydrologically based dataset of land surface fluxes and states for the conterminous United States: update and extensions. J Clim 26:9384–9392. https://doi.org/10.1175/jcli-d-12-00508.1
- Livneh B, Bohn TJ, Pierce DW, Munoz-Arriola F, Nijssen B, Vose R, Cayan DR, Brekke L (2015) A spatially comprehensive, hydrometeorological data set for Mexico, the U.S., and Southern Canada 1950–2013. ScieData 2:150042. https://doi.org/10.1038/sdata.2015.42
- Milly PCD, Betancourt J, Falkenmark M, Hirsch RM, Kundzewicz ZW, Lettenmaier DP, Stouffer RJ (2008) Stationarity is dead: whither water management? Science 319(5863):573–574. https://doi.org/10.1126/science.1151915
- Mishra V and Lettenmaier DP (2011). Climatic trends in major US urban areas, 1950–2009. Geophys Res Lett 38(16)
- Moss RH, Edmonds JA, Hibbard KA, Manning MR, Rose SK, van Vuuren DP, Carter TR, Emori S, Kainuma M, Kram T et al (2010) The next generation of scenarios for climate change research and assessment. Nature 463:747. https://doi.org/10.1038/nature08823
- Mote PW, Li S, Lettenmaier DP, Xiao M, Engel R (2018) Dramatic declines in snowpack in the western US npj. Clim Atmos Sci 1:2. https://doi.org/10.1038/s4292-018-0012-1
- Myers MR, Cayan DR, Iacobellis SF, Melack JM, Beighley RE, Barnard PL, Dugan JE and Page HM (2017). Santa Barbara area coastal ecosystem vulnerability assessment
- O'Neill JAI (2010) Climate change's impact on the design of water, wastewater, and stormwater infrastructure. Hydrol Days 2010:79–88
- Olsson J, Berggren K, Olofsson M, Viklander M (2009) Applying climate model precipitation scenarios for urban hydrological assessment: a case study in Kalmar City, Sweden. Atmos Res 92(3):364–375. https://doi. org/10.1016/j.atmosres.2009.01.015
- Orlowsky B, Seneviratne SI (2012) Global changes in extreme events: regional and seasonal dimension. Clim Chang 110(3):669–696
- Pierce DW, Barnett TP, Hidalgo HG, Das T, Bonfils C, Santer BD, Bala G, Dettinger MD, Cayan DR, Mirin A et al (2008) Attribution of declining Western U.S. snowpack to human effects. J Clim 21(23):6425–6444. https://doi.org/10.1175/2008jcli2405.1
- Pierce DW, Cayan DR, Thrasher BL (2014) Statistical downscaling using localized constructed analogs (LOCA). J Hydrometeorol 15(6):2558–2585
- Pierce DW, Cayan DR, Maurer EP, Abatzoglou JT, Hegewisch KC (2015) Improved bias correction techniques for hydrological simulations of climate change. J Hydrometeorol 16(6):2421–2442. https://doi.org/10.1175/jhm-d-14-0236.1
- Pierce DW, Kalansky JF and Cayan DR (2018). Climate, drought, and sea level rise scenarios for the fourth California climate assessment. California's Fourth Climate Change Assessment, California Energy Commission. Publication number: CNRA-CEC-2018-006
- Priestley CHB, Taylor RJ (1972) On the assessment of surface heat flux and evaporation using large-scale parameters. Mon Weather Rev 100(2):81–92. https://doi.org/10.1175/1520-0493(1972)100<0081:OTAOSH>2.3.CO;2
- Raoufi R, Beighley E (2017) Estimating daily global evapotranspiration using penman-monteith equation and remotely sensed land surface temperature. Remote Sens 9(11):1138
- Ray RL, Beighley RE, Yoon Y (2016) Integrating runoff generation and flow routing in Susquehanna River basin to characterize key hydrologic processes contributing to maximum annual flood events. J Hydrol Eng 21(9): 04016026. https://doi.org/10.1061/(ASCE)HE.1943-5584.0001389
- Rosenberg EA, Keys PW, Booth DB, Hartley D, Burkey J, Steinemann AC, Lettenmaier DP (2010) Precipitation extremes and the impacts of climate change on stormwater infrastructure in Washington state. Clim Chang 102(1):319–349. https://doi.org/10.1007/s10584-010-9847-0
- Schneider C, Laizé CLR, Acreman MC, Flörke M (2013) How will climate change modify river flow regimes in Europe? Hydrol Earth Syst Sci 17:325–339
- Swain DL, Langenbrunner B, Neelin JD, Hall A (2018) Increasing precipitation volatility in twenty-first-century California. Nat Clim Chang 8(5):427
- Tamaddun K, Kalra A, Ahmad S (2016) Identification of streamflow changes across the continental United States using variable record lengths. Hydrology 3(2):24
- Taylor KE, Stouffer RJ, Meehl GA (2012) An overview of CMIP5 and the experiment design. Bull Amer Meteor Soc 93:485–498. https://doi.org/10.1175/BAMS-D-11-00094.1
- Thakali R, Kalra A, Ahmad S (2016) Understanding the effects of climate change on urban stormwater infrastructures in the Las Vegas valley. Hydrology 3(4):34



- Thomas C. Peterson, Richard R. Heim, Robert Hirsch, Dale P. Kaiser, Harold Brooks, Noah S. Diffenbaugh, Randall M. Dole, Jason P. Giovannettone, Kristen Guirguis, Thomas R. Karl, Richard W. Katz, Kenneth Kunkel, Dennis Lettenmaier, Gregory J. McCabe, Christopher J. Paciorek, Karen R. Ryberg, Siegfried Schubert, Viviane B. S. Silva, Brooke C. Stewart, Aldo V. Vecchia, Gabriele Villarini, Russell S. Vose, John Walsh, Michael Wehner, David Wolock, Klaus Wolter, Connie A. Woodhouse, Donald Wuebbles, (2013) Monitoring and Understanding Changes in Heat Waves, Cold Waves, Floods, and Droughts in the United States: State of Knowledge. Bulletin of the American Meteorological Society 94(6):821–834
- Vano JA, Udall B, Cayan DR, Overpeck JT, Brekke LD, Das T, Hartmann HC, Hidalgo HG, Hoerling M, McCabe GJ et al (2014) Understanding uncertainties in future Colorado river streamflow. Bull Am Meteorol Soc 95(1):59–78. https://doi.org/10.1175/bams-d-12-00228.1
- Vicky E, Waliser DE, Bin G, Lavers DA, Martin RF (2018) Global analysis of climate change projection effects on atmospheric rivers. Geophys Res Lett 45(9):4299–4308. https://doi.org/10.1029/2017GL076968
- Warner MD, Mass CF, Salathé EPS Jr (2015) Changes in winter atmospheric rivers along the north american west coast in CMIP5 climate models. J Hydrometeorol 16(1):118–128. https://doi.org/10.1175/jhm-d-14-0080.1
- Warrick JA, Melack JM, Goodridge BM (2015) Sediment yields from small, steep coastal watersheds of California. J Hydrol: Regional Studies 4:516–534

Affiliations

Dongmei Feng ¹ • Edward Beighley ^{1,2} • Roozbeh Raoufi ¹ • John Melack ³ • Yuanhao Zhao ¹ • Sam Iacobellis ⁴ • Daniel Cayan ⁴

- Department of Civil and Environmental Engineering, Northeastern University, Boston, MA, USA
- Department of Marine and Environmental Science, Northeastern University, Boston, MA, USA
- ³ Bren School of Environmental Science and Management, University of California, Santa Barbara, CA, USA
- Scripps Institution of Oceanography, University of California, San Diego, CA, USA

